frontiers in Energy Research

ORIGINAL RESEARCH
published: 06 August 2021
doi: 10.3389/fenrg.2021.652239

# Anodic Performance of BaO-Added Ni/SDC for Solid Oxide Fuel Cell Fed With Dry $CH_4$

*Yoshiteru Itagaki*, Syuhei Yamaguchi and Hidenori Yahiro*

*Department of Materials Science and Biotechnology, Graduate School of Science and Engineering, Ehime University, Matsuyama, Japan*

SOFCs fed with dry $H_2$ and $CH_4$ fuels were examined using 20 wt% Ni/SDC and 0.2 wt% BaO-added 20 wt% Ni/SDC [Ni(BaO)/SDC] anodes. The i–v characteristics of the cells in $H_2$ and $CH_4$ resulted in a higher output produced by $CH_4$ fuel compared to that produced by $H_2$ fuel in both anodes. In both fuels, better anode characteristics were obtained for Ni(BaO)/SDC. Consequently, the anodic performance was in the order of Ni(BaO)/SDC in $CH_4$ > Ni/SDC in $CH_4$ > Ni(BaO)/SDC in $H_2$ > Ni/SDC in $H_2$. A significant carbon deposition was observed in the Ni/SDC anode in $CH_4$, but the carbon deposition observed in Ni(BaO)/SDC was less. From the DC electrical resistance measurement of the anode films, a remarkable decrease in resistance was observed in Ni/SDC due to the carbon deposition after $CH_4$ exposure. The resistance of Ni(BaO)/SDC was higher than that of Ni/SDC and did not change even after $CH_4$ exposure because of the less carbon deposit. The high dispersibility of Ni particles was confirmed in both anodes and was particularly remarkable in Ni(BaO)/SDC. The highest anodic performance in Ni(BaO)/SDC was attributed to the high Ni dispersibility which might promote $CH_4$ decomposition by producing less carbon deposit. It was speculated that the higher cell output in $CH_4$ than that in $H_2$ is due to the locally high concentration of $H_2$ and/or CO gas on the anode surface by the promotion of $CH_4$ decomposition.

**Keywords: SOFC, anode, Ni/SDC, BaO, $H_2$ and $CH_4$ fuels**

OPEN ACCESS

***Edited by:***
*Elisabetta Di Bartolomeo, University of Rome Tor Vergata, Italy*

***Reviewed by:***
*Aleksey Yaremchenko, University of Aveiro, Portugal*
*Massimiliano Lo Faro, National Research Council (CNR), Italy*

****Correspondence:***
*Yoshiteru Itagaki*
*itagaki.yshiteru.mj@ehime-u.ac.jp*

***Specialty section:***
*This article was submitted to Fuel Cells, a section of the journal Frontiers in Energy Research*

***Received:*** *12 January 2021*
***Accepted:*** *22 June 2021*
***Published:*** *06 August 2021*

***Citation:***
*Itagaki Y, Yamaguchi S and Yahiro H (2021) Anodic Performance of BaO-Added Ni/SDC for Solid Oxide Fuel Cell Fed With Dry $CH_4$. Front. Energy Res. 9:652239. doi: 10.3389/fenrg.2021.652239*

## INTRODUCTION

As solid oxide fuel cells (SOFCs) operate at high temperatures, they have the advantage of having higher power generation efficiency than the other fuel cells and can directly use different fuels other than hydrogen fuel ($H_2$). Methane ($CH_4$) is the main component of natural gas and is a raw material for hydrogen production by a steam reforming process. Single cell of SOFC was operated at 700°C, and at this temperature, $CH_4$ can be internally reformed in the cell without prereforming process. Many research studies on power generation by internal reforming of $CH_4$ using SOFC have been extensively performed (Son, 2002). The disadvantage of the internal reforming is the carbon deposit on an anode which reduces an anodic performance by closing the porous structure of the anode or powdering catalytic Ni particles (Finnerty et al., 1998). When $CH_4$ is used as a fuel, carbon deposition can be avoided by operating with a high steam/carbon ratio, S/C = 2–3. However, a high steam content simultaneously leads to dilution of the fuel. In this aspect, carbon-tolerant anodes in dry or low-steam-content $CH_4$ are desirable.

Ni/YSZ is used as a general-purpose anode material because Ni acts as a catalyst and an electron conduction path and YSZ acts as an oxide ion conducting phase. Ni/YSZ generally contains approximately 50–60 wt% Ni. However, a high concentration of Ni tends to promote coarsening of Ni particles during a chemical reaction at high temperature, thus causing high electrode overvoltage (Simwonis et al., 2000; Lee et al., 2002) and cell corruption because of volume expansion due to Ni reoxidation (Ettler et al., 2010). Ni-cermet anodes using Sm-doped ceria (SDC) have also demonstrated a good anodic performance in $H_2$ and $CH_4$ fuels (Zhang et al., 1999; Wang et al., 2003). In our previous work, we reported that high anodic performance can be obtained in dry $CH_4$ fuel using SDC chemically loaded with 20 wt % Ni (Asamoto et al., 2008). By reducing the amount of Ni, dispersed nanosized Ni particles are generated, and at reducing atmosphere, SDC develops mixed conductivity due to the reduction of $Ce^{4+}$ into $Ce^{3+}$, thus resulting in high anode characteristics. The 20 wt% Ni/SDC anode film formed by electrophoretic deposition (EPD) showed higher carbon resistance to dry $CH_4$ compared to the slurry-coated anode because a dense Ni/SDC film was formed using the EPD method, which improved oxide ionic conductivity in the anode film to effectively oxidize and remove the carbon deposit.

For the direct use of $CH_4$ in SOFCs, there are several reports on alkaline earth-modified Ni anodes that can be referred to. McIntyre et al. (2015) reported that 1% BaO-infiltrated Ni/YSZ anode in $CH_4$ effectively reduced carbon accumulation. Qu et al. (2016) also reported that CaO and BaO modifiers increase tolerance to carbon deposition. However, they both stated that the addition of BaO has a negative effect on the cell performance in $CH_4$.

The interaction between BaO and highly dispersed Ni can be expected to achieve both high carbon tolerance and electrochemical reaction activity even in $CH_4$ fuel. In this study, we evaluated anode characteristics in dry $H_2$ and $CH_4$ fuels using 20 wt% Ni/SDC with the addition of 0.2 wt% BaO, the effect of BaO addition on the anode structure and catalytic activity and the influence of carbon deposition under $CH_4$ fuel on the cell performance.

# EXPERIMENTAL

## Sample Preparation

Samaria-doped ceria, $(SmO_{1.5})_{0.2}(CeO_2)_{0.8}$ (SDC), was prepared using the method reported by Asamoto et al. (2008). The typical procedure is as follows. A mixed aqueous solution of $Sm(NO_3)_3{\cdot}6H_2O$ and $Ce(NO_3)_3{\cdot}6H_2O$ of stoichiometric molar ratio was added to an $NH_4OH$ solution. The resultant yellowish precipitate was filtrated and dried for 24 h; this was followed by calcination at 350°C for 4 h. SDC powders were ball-milled in ethanol for 24 h. The pulverized SDC powders were added to an aqueous solution of $Ni(NO_3)_2{\cdot}6H_2O$, and the mixture was stirred with a magnetic stirrer for one day. The dried powder of Ni-impregnated SDC was calcined at 700°C for 10 h. The loading amount of metallic Ni was fixed at 20 wt%. NiO/SDC powders containing BaO additive were prepared using a similar method, except for the use of a mixed solution of $Ni(NO_3)_2{\cdot}6H_2O$ and $Ba(NO_3)_2$ for impregnating SDC. The loading amounts of metallic Ni and BaO were 20 and 0.2 wt%, respectively. The resulting samples were characterized using X-ray diffusion (XRD) and field emission scanning electron microscopy (FE-SEM).

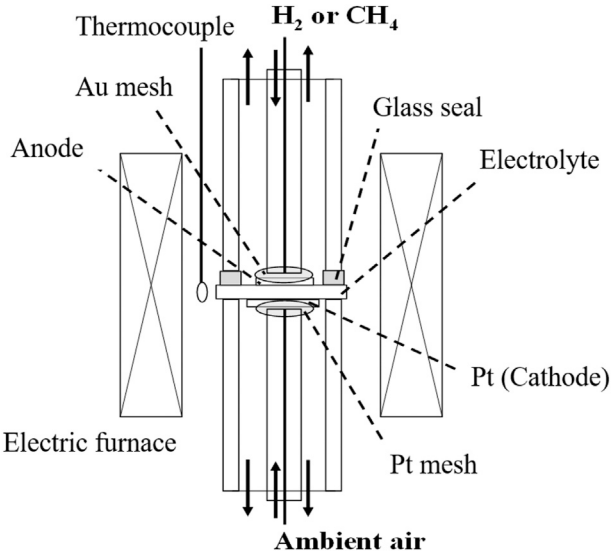


**FIGURE 1 |** Schematic picture of the configuration of the cell test under $H_2$ and $CH_2$ fuels.

## Fabrication of Single Fuel Cell

The powder, $(ScO_{1.5})_{0.20}(CeO_2)_{0.01}(ZrO_2)_{0.79}$ (ScCeSZ), was purchased from Tosoh Co. (Japan), as an electrolyte material. The ScCeSZ powders were uniaxially pressed into disks having an 8 mm diameter at 60 kgf·cm$^{-2}$ in a vacuum. The pressed disks were sintered at 1,500°C for 10 h to obtain a dense electrolyte disk. The thickness of the electrolyte after the sintering was 1.3 mm. The Pt electrode of the cathode having a 5.5 mm diameter was painted on one surface of the ScCeSZ electrolyte disk and heat-treated at 1,000°C for 20 min. The anode was fabricated on the opposite surface of the ScCeSZ electrolyte disk by an electrophoretic deposition (EPD) method. Details of the EPD method are reported in the study of Asamoto et al. (2008); the anode powder was suspended in iodine-added acetylacetone. The deposition surface of the ScCeSZ disk was coated with carbon. The anode deposited by EPD was heat-treated at 900°C for 5 h. The diameter of the anode was 3.5 mm.

## Measurement of i–v Characteristics

**Figure 1** illustrates the schematic view of the configuration of the fuel cell test. Gold and platinum meshes were used as the current collectors of the anode and cathode, respectively. The disk-type single cells were mounted on the top of an aluminum tube and sealed with a Pyrex glass. Before the fuel cell measurement, the glass seal was heated at 850°C, and then, the anode was exposed to a hydrogen atmosphere at 700°C for 1 h to reduce NiO to metallic Ni. For the fuel cell measurement, dry hydrogen or methane was introduced to the anode at a flow rate of 50 cm$^3$ min$^{-1}$. The

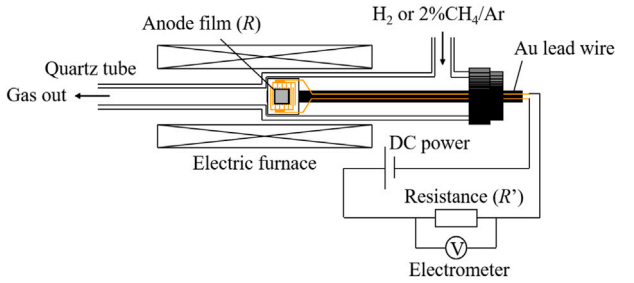


**FIGURE 2 |** The setup of DC resistance measurement for the anode films formed on the comb-type Au electrode under $H_2$ and 2%$CH_4$/Ar flow.

cathode was exposed to an ambient atmosphere. The measurement temperature of the fuel cell was 700°C. The i–v measurements were conducted under current control using carbon resistance elements connected in parallel to the cell; the terminal voltage of the resistance elements was measured using a digital multimeter. The i–v characteristics were measured twice and evaluated as the average value after confirming that the error was within 5%.

## Measurement of Catalytic Activity of Anode Materials

The reaction of methane on anode materials, Ni/SDC and Ni(BaO)/SDC, was examined using a conventional flow reactor. A physical mixture of 0.100 g of the sample (212–500 μm in particle size) and 0.300 g of quartz sand was set into a quartz tube having a 9 mm diameter. The sample was heated up to 900°C in helium and then reduced in hydrogen at the same temperature for 0.5 h. After this, the sample was flushed with helium to remove hydrogen and the reaction was started by supplying 1% methane and helium with a gas hourly space velocity (GHSV) of 20,000 $h^{-1}$. The reaction temperature and time were 700°C and 1 h, respectively. The effluent gases were analyzed using online gas chromatography with a thermal conductivity detector and a 3-m active carbon column. To analyze the deposited carbon, the Ni/SDC powder after the reaction was further examined with the temperature-programmed oxidation with $H_2O$ ($H_2O$-TPO). In this measurement, helium gas after passing through a $H_2O$ bubbler was fed in the carbon-deposited sample with a flow rate of 50 ml·$min^{-1}$. The reaction temperature was increased stepwise from 200 to 700°C. The activity was evaluated by the concentration of CO and $CO_2$. The reaction gas was analyzed with the TCD-GC similar to the aforementioned catalytic examination. To observe the deposited carbon directly, the anode powders pressed into disks treated with methane similar to the aforementioned catalytic examination and cross section of the disks after the $CH_4$ treatment were observed by SEM-EDS.

## Measurement of Sample Resistance

The electrical resistance of the anode film was measured as follows. **Figure 2** shows the schematic view of the measurement device. The anode film was deposited using the EPD method on a comb-type Au electrode printed on an $Al_2O_3$ substrate. The sample was placed into a quartz tube and heated to 850°C at a heating rate of 5°C $min^{-1}$, and then, 2% $CH_4$/Ar gas was introduced at 700°C for 1 h. Electrical resistance was measured in Ar. In the external circuit, DC power (10 V) and the reference resistance, $R$' (100 Ω–33 MΩ), were connected in series, and the terminal voltage, $E$', at the resistance was measured using an electrometer. The resistance of the elements, $R$, was determined by the following equation: $R = (10\text{-}E')R'/E'$.

# RESULTS AND DISCUSSION

## i–v Characteristics of the Cells with Ni/SDC and Ni(BaO)/SDC Anodes in $H_2$ and $CH_4$

**Figure 3** shows the XRD patterns of the powder samples before and after $H_2$ reduction. The SDC powder prepared at 350°C exhibited broad signals, suggesting that calcination at a low temperature produced a fine particle size of SDC. Crystallite sizes of the SDC particles were evaluated using the Scherrer equation which is as follows:

$$D = \frac{K\lambda}{B\cos\theta}, \quad (1)$$

where $D$ is the crystallite size (nm), $K$ is the Scherrer constant (0.90), $\lambda$ is the wavelength of X-ray (Cu–Kα 0.154 nm), and $B$ and $\theta$ are the FWHM (rad) and Bragg angle (rad) of the relevant XRD peak, respectively. Crystallite sizes of the SDC particles in the Ni-unloaded SDC, Ni/SDC, and Ni(BaO)/SDC were evaluated to be 4.6, 13.2, and 12.2 nm, respectively. For the Ni- and Ni(BaO)-impregnated samples, the dual phases of NiO/SDC and Ni/SDC were observed before and after the $H_2$-reduction process, respectively. No diffraction peaks of BaO in the Ni(BaO)/SDC sample were observed because of the small amount of BaO supported (0.2 wt%). After $H_2$ reduction, NiO was completely reduced to metallic Ni in the NiO-supported SDC samples.

**Figure 4** shows the i–v and i–p characteristics of a cell with a Ni/SDC anode when operated under the supply of $H_2$ fuel (A) and $CH_4$ fuel (B). Open circuit voltages (OCV) in the two fuels are 1.27 V (Ni/SDC) and 1.27 V (Ni(BaO)/SDC) for $H_2$ fuel and 1.28 V (Ni/SDC) and 1.33 V (Ni(BaO)/SDC) for $CH_4$ fuel. The OCV value with Ni(BaO)/SDC in $CH_4$ was specifically higher than the others. Adding 0.2 wt% BaO to Ni/SDC significantly enhanced the cell performance in both fuels; the maximum power density was 35 $mWcm^{-2}$ in $H_2$ fuel and 61 $mWcm^{-2}$ in $CH_4$ fuel. Consequently, the anodic performance was in the order of Ni(BaO)/SDC in $CH_4$ > Ni/SDC in $CH_4$ > Ni(BaO)/SDC in $H_2$ > Ni/SDC in $H_2$. Notably, significant carbon deposition was observed on the Ni/SDC anode after cell operation in $CH_4$ fuel, but the carbon deposition was suppressed in the case of the Ni(BaO)/SDC anode.

Better cell performance was obtained in dry $CH_4$ fuel compared to that in $H_2$ fuel with both anodes. In $CH_4$ fuel, the following anodic reactions were considered:

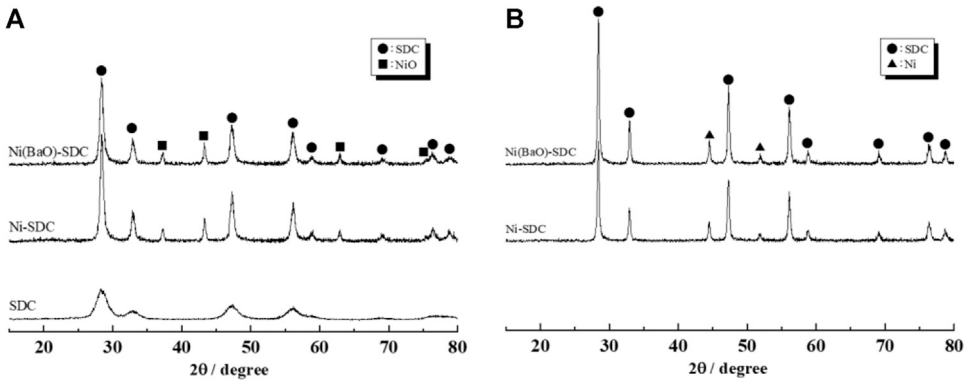


**FIGURE 3 |** XRD patterns of anode powders before **(A)** and after **(B)** $H_2$ reduction. The SDC powder **(A)** was calcined at 350°C, and Ni/SDC and Ni(BaO)/SDC powders were fired at 700°C. The powders **(B)** were subsequently reduced in $H_2$ at 700°C.

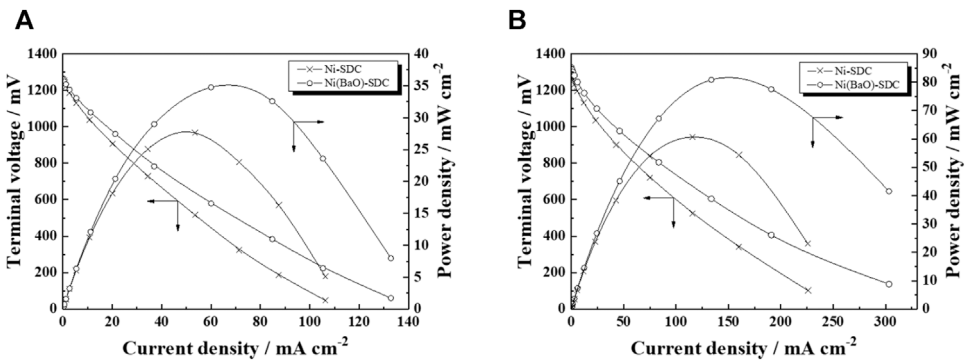


**FIGURE 4 |** The i–v and i–p characteristics of the cells with Ni/SDC and Ni(BaO)/SDC anodes at 700°C in $H_2$ **(A)** and $CH_4$ **(B)** fuels.

$$CH_4 = 2H_2 + C, \quad (2)$$

$$C + 2O^{2-} = CO_2 + 4e^-, \quad (3)$$

$$C + O^{2-} = CO = 2e^-, \quad (4)$$

$$CH_4 + 4O^{2-} = CO_2 + 2H_2O + 8e^-, \quad (5)$$

$$CH_4 + O^{2-} = CO + 2H_2 + 2e^-, \quad (6)$$

$$CO + O^{2-} = CO_2 + 2e^-, \quad (7)$$

$$H_2 + O^{2-} = H_2O + 2e^-. \quad (8)$$

In $CH_4$ fuel, if the $CH_4$ cracking reaction **(2)** occurs near the surface of the anode, reaction **(8)** is a possible electrochemical reaction, as in the case of $H_2$ fuel. Noncracking processes, reactions **(5)**–**(7)**, are also expected. It is deduced that reaction **(8)** subsequently to $CH_4$ cracking is the main process on the Ni/SDC anode because it exhibited significant carbon deposition. Since carbon deposition is suppressed in the Ni(BaO)/SDC anode, carbon oxidation processes **(3)**–**(4)** would be expected in addition to the noncracking processes **(5)**–**(7)**. Alipour et al. (2014) reported that adding alkali metal oxide to $Ni/Al_2O_3$ catalyst is effective for enhancing the catalytic activity of dry $CH_4$ reforming. They concluded that adding alkali metal decreased the surface area of the catalyst but increased the reducibility of NiO into metallic Ni, which induced oxidative carbon illumination. Jing et al. (2004) reported that adding BaO to $Ni/SiO_2$ catalyst enhanced Ni dispersion on support, inducing the high catalytic activity of dry reforming and partial oxidation of $CH_4$. In both cases, it seems that the addition of alkali metals promotes carbon removal by directly interacting with Ni particles. **Figure 5** shows the catalytic $CH_4$ conversion on the two anode catalysts under the $CH_4$ stream. No significant difference in activity was observed between the two catalysts, and almost 100% conversion rate was maintained at 700°C for 1 h, suggesting that the two anodes have sufficient catalytic activity for methane conversion. Therefore, the less carbon deposition in Ni(BaO)/SDC is not due to less $CH_4$ conversion but fast consumption of produced carbon.

## Resistance of Anode Films after $H_2$ and $CH_4$ Treatment

Jaiswal et al. (2014) reported that CaO- and SrO-doped ceria, $Ce_{0.93}Ca_{0.05}Sr_{0.02}O_{2-\delta}$, exhibited high ionic conductivity in air. They explain the increase in conductivity from the following perspectives: increased number of oxygen defects due to divalent

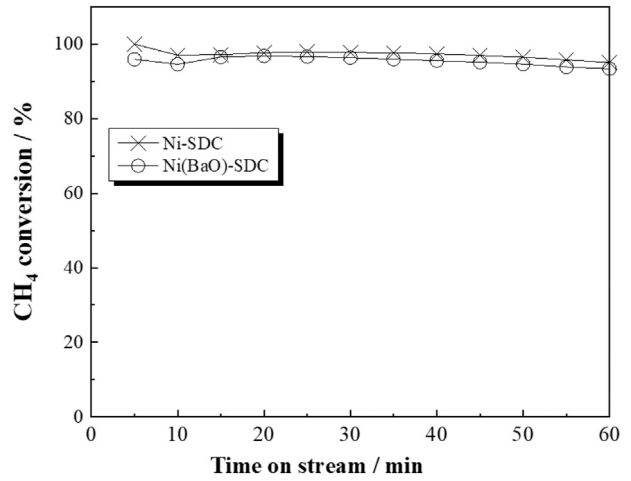


**FIGURE 5 |** Time on the steam of catalytic $CH_4$ conversion of the Ni/SDC and Ni(BaO)/SDC powders measured under 1% $CH_4$/He flow with GHSV = 20,000 $h^{-1}$ at 700°C.

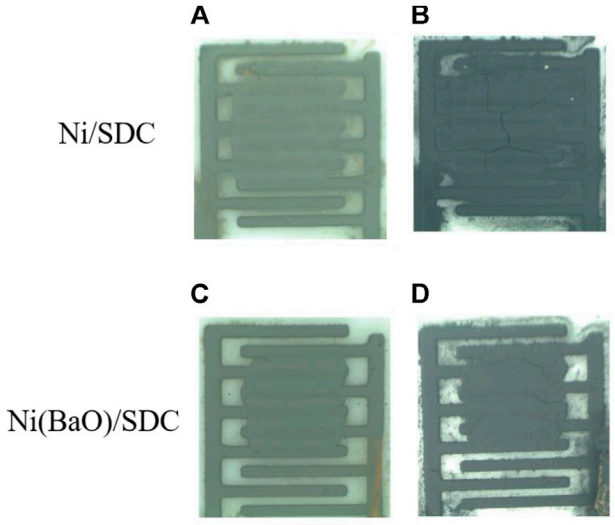


**FIGURE 7 |** Appearance of the surfaces of the Ni/SDC and Ni(BaO)/SDC films formed on a comb-type Au electrode by EPD after $H_2$ reduction **(A)** and **(C)** and after further $CH_4$ exposure **(B)** and **(D)**.

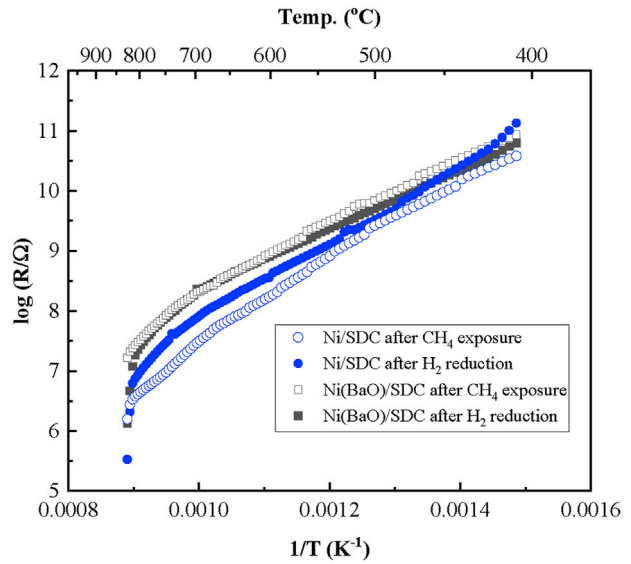


**FIGURE 6 |** Temperature dependence of electrical resistance of the Ni/SDC and Ni(BaO)/SDC films formed on a comb-type Au electrode by EPD. The measurements were conducted in an Ar atmosphere after $H_2$ reduction and after further exposure in $CH_4$ at 700°C.

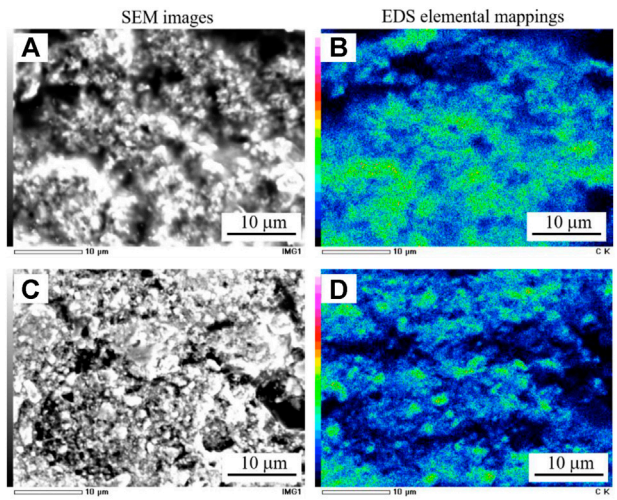


**FIGURE 8 |** Cross-sectional SEM and EDS images of the anode disks exposed with methane at 700°C for 1 h: SEM images **(A)** Ni/SDC and **(C)** Ni(BaO)/SDC, and carbon elemental mappings **(B)** Ni/SDC and **(D)** Ni(BaO)/SDC.

ion doping, scavenging of impurities present at grain boundaries by alkali metals, and decrease in grain boundary resistance of fine ceria particles induced by doping.

The anode films were formed on a comb-type Au electrode and the electrical resistance was measured. **Figure 6** shows the temperature-dependent resistance changes of the Ni/SDC and Ni(BaO)/SDC films in Ar after $H_2$ reduction and further treatment under $CH_4$ gas flows. As shown in the figure, a semiconductor-like behavior was observed in which the resistance value decreased with the increasing temperature in the electrode films, irrespective of the presence or absence of BaO. As a result, the Ni(BaO)/SDC anode exhibited a higher resistance compared to Ni/SDC anode. Therefore, it is deduced that the added BaO acts as an insulating phase rather than interacting with the Ni particles.

In the $CH_4$ treatment, the resistance did not significantly change in Ni(BaO)/SDC but remarkably decreased in Ni/SDC. In general, it is thought that the carbon deposition at an anode leads to the deterioration of cell performance by reducing TPB

**TABLE 1 |** Activation energies of electric conduction of the anode films formed on the comb-type Au electrode. The values were evaluated from the temperature-dependent resistance in Ar subsequently to the $H_2$ or 2% $CH_4$/Ar exposure.

| Anode | Gas treatment | Activation energy (eV) | |
|---|---|---|---|
| | | Above 650°C | Below 650°C |
| Ni/SDC | $H_2$ | 1.57 | 1.34 |
| | $CH_4$ | 1.78 | 1.33 |
| Ni(BaO)/SDC | $H_2$ | 1.47 | 1.04 |
| | $CH_4$ | 1.43 | 1.12 |

length and closing the molecular diffusion path. Controversially, it has also been reported that deposited graphitic carbon improves the conductivity of the electrode (MacIntosh et al., 2004; Li et al., 2015a). MacIntosh et al. (2004) reported that carbon deposited over the Cu-YSZ anode improved the conductivity near the TPB and increased cell output. Since the Ni metal phase fraction is only 20 wt%, which is not sufficient to form an electron conduction path, the decreased resistance of Ni/SDC from $CH_4$ exposure is possibly related to the carbon deposition formed by reaction **(2)** over the film. The surface appearances of the anode films on the comb-type Au electrode before and after the $CH_4$ treatment are shown in **Figure 7**. Although the carbon deposition was confirmed in both films, it was much less pronounced in the Ni(BaO)/SDC film, suggesting the fed $CH_4$ and/or deposited carbon are oxidized. **Figure 8** shows the cross-sectional SEM images and EDS elemental mappings of carbon in the Ni/SDC and Ni(BaO)/SDC disks after the methane treatment at 700°C for 1 h. The elemental mappings clearly indicated that the Ni/SDC anode contains a larger amount of carbon deposit than the Ni(BaO)/SDC anode.

It is reasonable to say that the resistance did not change in the Ni(BaO)/SDC film that yields a smaller amount of carbon deposition compared to the Ni/SDC film. Note that there is no oxygen supply from the feed gas in this experiment, and the oxidation of $CH_4$ and/or carbon occurs through surface oxygen of the anode and/or with produced oxides such as $H_2O$, CO, and $CO_2$. Garía et al. (2010) reported on methane oxidation using the lattice oxygen of $Ni/BaTi_{1-x}In_xO_{3-\delta}$ perovskite-type oxide in the absence of atmospheric oxygen. They concluded that the oxidation process is related to a surface oxygen species reaction that generates oxygen vacancy. The oxygen vacancy is readily produced due to the high reducibility of the $In^{3+}$ B-site ion, which is replenished by oxygen diffusion from bulk. SDC used in this study is characterized by the high reducibility of $Ce^{4+}$ to $Ce^{3+}$ and oxide ionic conductivity. Since the BaO-doped anode specifically suppressed carbon deposition, the interaction between SDC and BaO and/or Ni and BaO may become significant. **Figure 6** shows the Arrhenius plot with log (σT/S·K) on the vertical axis for the result in **Figure 6**. The slopes of the plots change around 650°C, suggesting that the conduction mechanism differs between the high- and low-temperature regions. **Table 1** shows the activation energies obtained from

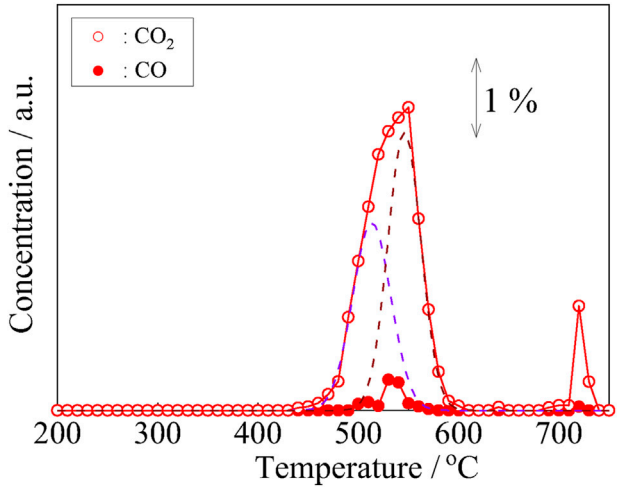


**FIGURE 9 |** Temperature-programmed oxidation under a humidified He flow ($H_2O$-TPO) for the Ni/SDC powder after the $CH_4$ treatment at 700°C for 1 h. TPO condition He gas after passing through a $H_2O$ bubbler at a flow rate of 50 ml·min$^{-1}$. The reaction temperature increased from 200 to 700°C with the rate of 1°C min$^{-1}$.

the linear fit of the plots evaluated for the two temperature regions, that is, above and below 650°C. The values of Ni/SDC seem to be larger than those of Ni(BaO)/SDC. Besides, by comparing the two gases, the activation energy is higher after $CH_4$ exposure than after hydrogen exposure. Wright and Virkar (2011) measured the conductivity of porous SDC as a function of temperature and oxygen partial pressure. They concluded that oxide ion transport is predominant below 300°C, but electron conduction occurs above 400°C in reducing atmosphere; the estimated activation energy is 73,890 J·mol$^{-1}$ (0.766 eV) for the oxide ion transport and 101,050 J·mol$^{-1}$ (1.05 eV) for mixed conduction. It is accepted that doped ceria expresses electronic conduction in reducing atmosphere based on the reduction of $Ce^{4+}$ into $Ce^{3+}$ (Yahiro et al., 1989; Shimonosono et al., 2004). In the present cases, both Ni/SDC and Ni(BaO)/SDC are, therefore, thought to be in a mixed conduction state in an Ar atmosphere. Focusing on the higher temperature region (> 650°C), the activation energies in this study are higher than those reported by Wright and Virkar (2011). Considering that the influence of SDC on electrical conductivity is dominant, it is considered that the anode films also show mixed conductivity at a high temperature, but the high activation energy is due to the intergranular resistance between SDC particles. However, Ni/SDC after exposure to $CH_4$ shows specifically high activation energy compared to the other cases. The deposited carbon may be predominant in the Ni/SDC anode.

To identify the carbon species deposited on the electrode, temperature-programmed oxidation (TPO) profile was monitored on the $CH_4$-treated anode powders under the flow of Ar-$H_2O$ gas ($H_2O$-TPO). The result of the Ni/SDC powder is shown in **Figure 9**. Two oxidated species, $CO_2$ and CO, were observed. Concerning $CO_2$, two peaks were distinctly observed at approximately 550 and 700°C. The lower temperature peak is

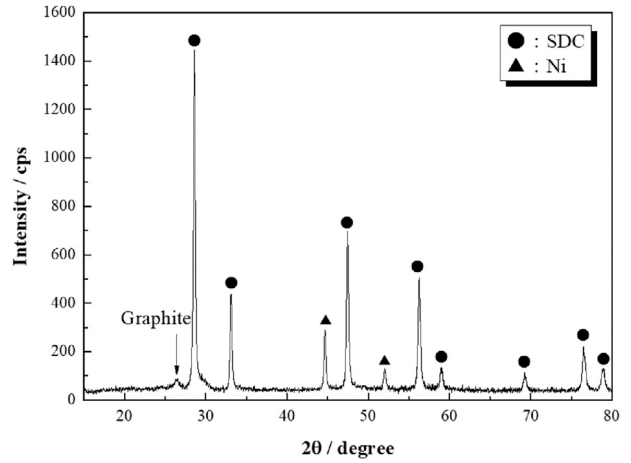


**FIGURE 10 |** XRD pattern of the Ni/SDC powder after $CH_4$ exposure at 700°C.

attributable to the oxidation of amorphous carbon species, and the higher temperature peak is associated with fibrous carbon or graphitic carbon (Skalar et al., 2016). The existence of graphite was also confirmed by the peak at 2θ = 26.6 in the XRD pattern (JCPDS file no. 75-1621) shown in **Figure 10**. The lower temperature peak with an asymmetrical shape was further deconvoluted as the two dotted curves shown in **Figure 9**. These peaks were assigned to the high and low degrees of amorphous carbons (Skalar et al., 2016). The reduced resistance of Ni/SDC by $CH_4$ exposure is due to the deposited amorphous and graphitic carbons forming electron conduction paths.

## High Performance of the Ni(BaO)/SDC Anode in $CH_4$

Both anodes exhibited a better performance when fueled with $H_2$ compared to when fueled with $CH_4$. In fact, the performance in $H_2$ is not absolutely high even in Ni(BaO)/SDC: the maximum power density was no more than 35 $mWcm^{-2}$ in $H_2$. Conductivity in 20 wt% Ni content is not as high as conventional anodes such as 50–60 wt% Ni-YSZ that possesses more than $10^3$ S $cm^{-1}$. Even though SDC exhibits electronic conductivity no more than $10^{-1}$ S $cm^{-1}$ at 700°C (Yahiro et al., 1989), the low performance might be due to the low conductivity of 20 wt% Ni/SDC. McIntyre et al. (2015) evaluated the single cell in $H_2$ at 730°C with 50 wt% Ni-YSZ cermet and YSZ electrolyte with a thickness of 0.6 mm. The maximum output is almost equivalent to the present case. Therefore, the thickness of the electrolyte is possibly the reason for the low performance in $H_2$ and the low conductivity of 20 wt% Ni/SDC.

It has been reported that adding Ba or other alkali-earth metal leads to a low amount of carbon deposition. The elimination of carbon deposition is usually related to the steam reforming process.

$$C + H_2O = CO + H_2. \quad (9)$$

In this process, interfaces between Ba and Ni or Ba and SDC enhances the reaction of carbon with $H_2O$, which shift the equilibrium of $CH_4$ oxidation reaction to the right side of the reaction scheme **(2)**. The loaded Ba would be easily oxidized into BaO or BaOH by formed $H_2O$ acting as an adsorption site of $H_2O$ to catalyze the reaction of carbon elimination as reported by Yang et al. (2011). Islam and Hill (2013) also reported the positive effect of BaO addition in 50 wt% Ni/YSZ on the cell performance in dry $CH_4$ fuel. They explained that the added 5% BaO helped in $H_2O$ gasification of the carbon deposits. A similar effect of suppressing carbon deposition was observed, in this study, for 0.2 wt% BaO-added 20 wt% Ni/SDC. To elucidate the effect of BaO addition to Ni/SDC, Ni particle morphologies were directly observed by FE-SEM EDS. **Figure 11** shows FE-SEM photographs of Ni/SDC and Ni(BaO)/SDC powders after the $H_2$ reduction treatment, along with Ni element mapping images by EDS. From the elemental mappings, particle diameter was directly evaluated for the randomly sampled 100 Ni particles in the EDS mappings. **Figure 11** also shows the Ni particle size distributions on Ni/SDC and Ni(BaO)/SDC powders. Ni(BaO)/SDC exhibits a monodispersed distribution of approximately 50 nm. The mean values evaluated from the measurement are 73 nm for Ni/SDC and 59 nm for Ni(BaO)/SDC. It is thus confirmed that Ni particles are highly dispersed on both the anodes, and it is more effective by the BaO addition. This high dispersion of Ni particles undoubtedly promotes the catalytic activity on the anode, though activation of reaction **(2)** causes carbon deposition. Carbon deposit would be removed by the direct oxidation with reaction **(3)** or **(4)**, and in this case, $O^{2-}$ would be supplied from the SDC phase in the anode. Since both Ni/SDC and Ni(BaO)/SDC are mainly composed of SDC acting as a $O^{2-}$ conductor, reactions **(3)**–**(4)** cannot explain the less carbon deposition in Ni(BaO)/SDC. The contribution of $H_2O$ formed by reaction **(5)** or **(8)** to suppress carbon deposition should be also considered in the present case. In the i–v characteristics in **Figure 4**, OCV of Ni(BaO)/SDC in $CH_4$ is 1.33 V, which is characteristically large compared to other cases. This specifically high OCV of Ni(BaO)/SDC may suggest that the three-phase boundaries of the anode are rich in hydrogen originated from the $CH_4$ decomposition. However, the anodic performance of Ni(BaO)/SDC in $H_2$ is higher than that of Ni(BaO)/SDC, still lower than that of 50 wt% Ni/YSZ reported by Islam and Hill (2013). The major difference in those anodes is the Ni content. Though SDC exhibits a significant electronic conductivity in reducing atmosphere, it is no more than in the level of $10^{-1}$ S $cm^{-1}$ at 700°C (Yahiro et al., 1989). Besides, 20 wt% Ni content is under the percolation limit (Lee et al., 2002), and therefore, the 20 wt% Ni/SDC has a lower conductivity compared to 50 wt% Ni/YSZ. The carbon deposit seen in $CH_4$ fuel might act as a current collector, which compensates the lack of conductivity of the Ni/SDC. However, Ni(BaO)/SDC does not yield carbon deposit enough to decrease its resistance as shown in **Figure 6**. The cause of the superiority of $CH_4$ fuel over hydrogen fuel in Ni(BaO)/SDC is still unclear and further investigation is required. If the decomposition of methane with reaction **(1)**

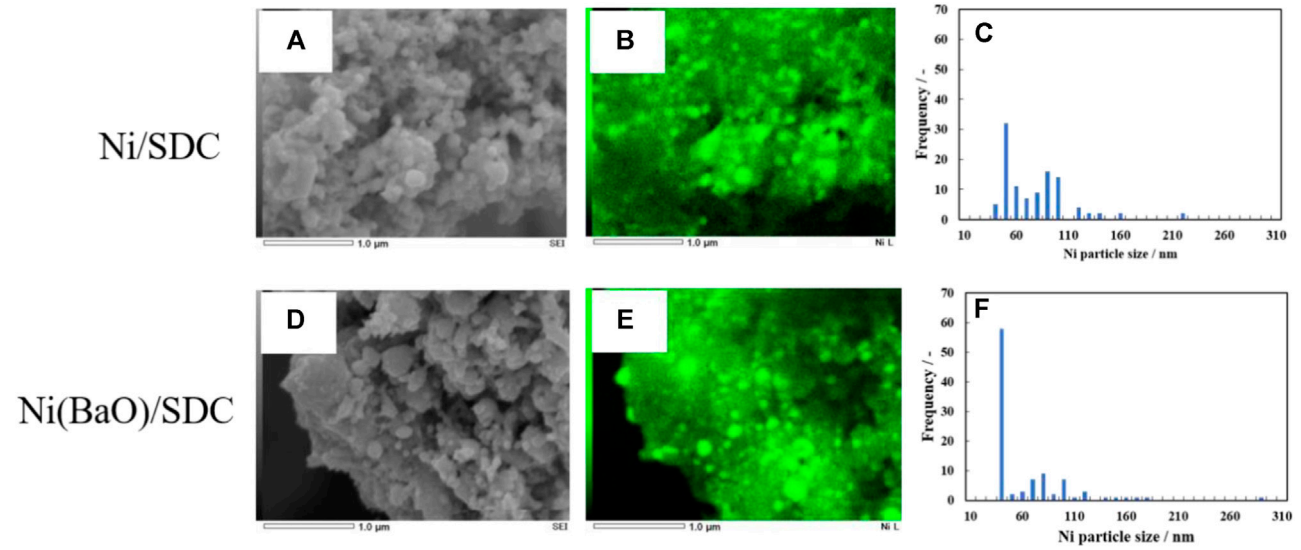


**FIGURE 11 |** FE-SEM pictures **(A,D)**, EDS elemental mappings of Ni within the FE-SEM images **(B,E)**, and particle size distributions of Ni scaled directly for randomly sampled 100 Ni particles in the EDS mappings **(C,F)**.

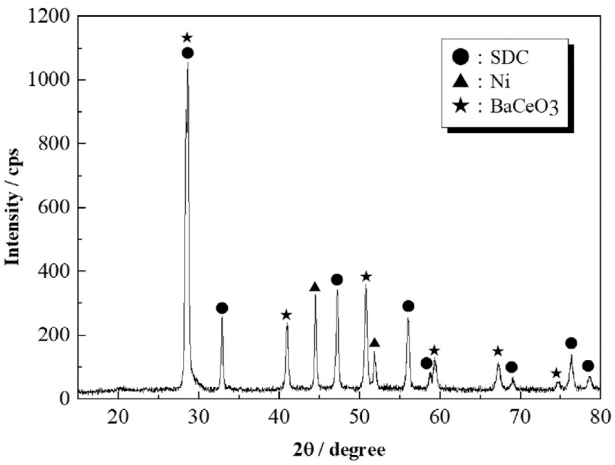


**FIGURE 12 |** XRD pattern of the 20wt% BaO-added Ni/SDC powder fired at 700°C and reduced in $H_2$ at 900°C.

and the removal of carbon by water are very fast, the anode should be locally exposed to a high concentration of $H_2$ and CO gases. This could be expected as one of the reasons for the superiority of $CH_4$ fuel in Ni(BaO)/SDC.

## The Effect of BaO Addition on Ni Particle Dispersion

It is deduced that a small amount of BaO-added interacts with Ni particles and effectively induces Ni particle dispersion, which increases TPB length. It has been reported that the interaction between BaO and Ni modifies carbon tolerance (Islam and Hill, 2013; Rosa et al., 2009; Yang et al., 2011). Yang et al. (2011) reported the formation of nanointerface of BaO/Ni, where nanosized BaO islands grow on the Ni surface. They concluded that the nanointerface provides a water adsorption site for the deposited carbon oxidation. In this study, BaO could not be directly observed in the FE-SEM EDS mapping, but the similar structure of BaO/Ni may have enhanced the anodic reactions. Meanwhile, BaO/SDC interface should also be considered. As mentioned above, the addition of BaO to Ni/SDC enlarged the electrical resistance in Ar gas. BaO possibly reacts with SDC to form $Ba(Ce,Sm)O_3$ phase at the interface. Since the amount of BaO is as small as 0.2 wt%, this reaction phase could not be detected. To detect the reaction phase, BaO content was increased to 20 wt%. **Figure 12** shows the XRD pattern of 20 wt% BaO-added Ni/SDC powder. The $BaCeO_3$ [or $Ba(Ce,Sm)O_3$] phase was detected together with Ni and SDC phases. This perovskite oxide is known as a protonic conductor but is less conductive in terms of oxide ion and electron in reducing conditions (Guan et al., 1997; Ma et al., 1998); although oxide ionic conductivity is dominant at high temperatures in $O_2/H_2O$, its conductivity is smaller than an order of magnitude than that of SDC (Inaba and Tagawa, 1996). Therefore, if the perovskite layer is formed at the interface, it acts rather as an insulating phase. If the perovskite phase forms near the Ni phase, a new interface, $Ni/BaCeO_3$, would be achieved. Carbon-tolerant Ni-based cermet anodes using the proton-conducting perovskite oxides have been reported by several researchers (Shimada et al., 2013; Li et al., 2015b). Li et al. (2015a) examined Y-(BCY) and Yb-doped barium cerates (BCYb) impregnated into $Ni/Gd_2O_3$-$CeO_2$ in wet $CH_4$ fuel. They concluded that BCY and BCYb adsorb and split water that effectively reacts with the deposited carbon. Although dry $CH_4$ was used in this

study, the water produced might also contribute to carbon elimination.

## CONCLUSION

20 wt% Ni/SDC and 0.2 wt% BaO-doped 20 wt% Ni/SDC [Ni(BaO)/SDC] were examined as anodes of SOFCs fed with dry $H_2$ and $CH_4$ fuels. The Ni(BaO)/SDC anode exhibited significantly higher performance in both fuels compared to the Ni/SDC anode. In particular, the anodic performance in $CH_4$ was higher than that in $H_2$. Electrical resistance was measured after hydrogen exposure of the anode film and further after $CH_4$ exposure. A significant carbon deposition was observed in the Ni/SDC film exposed to $CH_4$, and the electrical resistance of the film decreased accordingly owing to the carbon deposit forming a conductive phase on the anode. Although the addition of BaO increased the electrical resistance of Ni/SDC, the amount of carbon deposition was small, and the electrical resistance after $CH_4$ exposure did not change from that after $H_2$ exposure. Since the addition of BaO further improved the dispersibility of Ni particles, the electrochemical reaction fields of $H_2$ and $CH_4$ are increased, and the deposited carbon is efficiently removed by $H_2O$ at the Ni/BaO interface and/or at the interface between the $BaCeO_3$ or $Ba(Ce,Sm)O_3$ phase formed on the SDC surface. Further investigation is required to elucidate the superiority of $CH_4$ compared to $H_2$ on Ni(BaO)/SDC, but the enrichment of fuel gas such as $H_2$ and CO on the electrode due to the highly activated decomposition of $CH_4$ and carbon removal is considered to be a possible reason. Further examinations are currently conducted for the long-term stability of the cell performance and catalytic activity of the Ni(BaO)/SDC electrode in a dry methane condition.

## DATA AVAILABILITY STATEMENT

The original contributions presented in the study are included in the article/Supplementary Material; further inquiries can be directed to the corresponding author.

## AUTHOR CONTRIBUTIONS

YI analyzed experimental data of the anodic properties. SY prepared the anode catalysts and made their characterizations. HY made a theoretical interpretation of the data of catalytic functions.

## FUNDING

Subsidy supported by JSPS KAKENHI Grant Number 16K06774.

## ACKNOWLEDGMENTS

This work was conducted as a part of the Research Unit for Power Generation and Storage Materials (PGeS) at Ehime University.

## REFERENCES

Alipour, Z., Rezaei, M., and Meshkani, F. (2014). Effect of Alkaline Earth Promoters (MgO, CaO, and BaO) on the Activity and Coke Formation of Ni Catalysts Supported on Nanocrystalline Al2O3 in Dry Reforming of Methane. *J. Ind. Eng. Chem.* 20, 2858–2863. doi:10.1016/j.jiec.2013.11.018

Asamoto, M., Miyake, S., Itagaki, Y., Sadaoka, Y., and Yahiro, H. (2008). Electrocatalytic Performances of Ni/SDC Anodes Fabricated with EPD Techniques for Direct Oxidation of CH4 in Solid Oxide Fuel Cells. *Catal. Today* 139, 77–81. doi:10.1016/j.cattod.2008.08.027

Ettler, M., Timmermann, H., Malzbender, J., Weber, A., and Menzler, N. H. (2010). Durability of Ni Anodes during Reoxidation Cycles. *J. Power Sourc.* 195, 5452–5467. doi:10.1016/j.jpowsour.2010.03.049

Finnerty, C. M., Coe, N. J., Cunningham, R. H., and Ormerod, R. M. (1998). Carbon Formation on and Deactivation of Nickel-Based/zirconia Anodes in Solid Oxide Fuel Cells Running on Methane. *Catal. Today* 46, 137–145. doi:10.1016/S0920-5861(98)00335-6

García, V., Caldes, M. T., Joubert, O., Gautron, E., Mondragon, F., and Moreno, A. (2010). Methane Oxidation by Lattice Oxygen of $Ni/BaTi_{1-x}In_xO_{3-\delta}$ Catalysts. *Catal. Today* 157, 177–182. doi:10.1016/j.cattod.2010.01.021

Guan, J., Dorris, S. E., Balachandran, U., and Liu, M. (1997). Transport Properties of BaCe0.95Y0.05O3−α Mixed Conductors for Hydrogen Separation. *Solid State Ionics* 100, 45–52. doi:10.1016/S0167-2738(97)00320-2

Inaba, H., and Tagawa, H. (1996). Ceria-based Solid Electrolytes. *Solid State Ionics* 83, 1–16. doi:10.1016/0167-2738(95)00229-4

Islam, S., and Hill, J. M. (2013). Barium Oxide Promoted Ni/YSZ Solid-Oxide Fuel Cells for Direct Utilization of Methane. *J. Mater. Chem. A.* 2, 1922–1929. doi:10.1039/c3ta12381b

Jaiswal, N., Kumar, D., Upadhyay, S., and Parkash, O. (2014). Ceria Co-doped with Calcium (Ca) and Strontium (Sr): a Potential Candidate as a Solid Electrolyte for Intermediate Temperature Solid Oxide Fuel Cells. *Ionics* 20, 45–54. doi:10.1007/s11581-013-0936-8

Jing, Q., Lou, H., Mo, L., Fei, J., and Zheng, X. (2004). Combination of CO2 Reforming and Partial Oxidation of Methane over Ni/BaO-SiO2 Catalysts to Produce Low H2/CO Ratio Syngas Using a Fluidized Bed Reactor. *J. Mol. Catal. A: Chem.* 212, 211–217. doi:10.1016/j.molcata.2003.10.041

Lee, J., Moon, H., Lee, H.-W., Kim, J., and Yoon, K.-H. (2002). Quantitative Analysis of Microstructure and its Related Electrical Property of SOFC Anode, Ni-YSZ Cermet. *Solid State Ionics* 148, 15–26. doi:10.1016/S0167-2738(02)00050-4

Li, M., Hua, B., Luo, J.-l., Jiang, S. P., PuChi, J. B., Chi, B., et al. (2015b). Carbon-tolerant Ni-Based Cermet Anodes Modified by Proton Conducting Yttrium- and Ytterbium-Doped Barium Cerates for Direct Methane Solid Oxide Fuel Cells. *J. Mater. Chem. A.* 3, 21609–21617. doi:10.1039/C5TA06488K

Li, P., Zhao, Y., Yu, B., Li, J., and Li, Y. (2015a). Improve Electrical Conductivity of Reduced La 2 Ni 0.9 Fe 0.1 O 4+δ as the Anode of a Solid Oxide Fuel Cell by Carbon Deposition. *Int. J. Hydrogen Energ.* 40, 9783–9789. doi:10.1016/j.ijhydene.2015.06.026

Ma, G., Shimura, T., and Iwahara, H. (1998). Ionic Conduction and Nonstoichiometry in BaxCe0.90Y0.10O3−α. *Solid State Ionics* 110, 103–110. doi:10.1016/S0167-2738(98)00130-1

MacIntosh, S., He, H., Lee, S-I., Costa-Nunes, O., Krishnan, V., Vohs, J. M., et al. (2004). An Examination of Carbonaceous Deposits in Direct-Utilization SOFC Anodes. *J. Electrochem. Soc.* 151, A604–A608. doi:10.1149/1.1650837

McIntyre, M. D., Kirtley, J. D., Singh, A., Islam, S., Hill, J. M., and Walker, R. A. (2015). Comparing *In Situ* Carbon Tolerances of Sn-Infiltrated and BaO-Infiltrated Ni-YSZ Cermet Anodes in Solid Oxide Fuel Cells Exposed to Methane. *J. Phys. Chem. C* 119, 7637–7647. doi:10.1021/acs.jpcc.5b01345

Qu, J., Wang, W., Chen, Y., Deng, X., and Shao, Z. (2016). Stable Direct-Methane Solid Oxide Fuel Cells with Calcium-Oxide-Modified Nickel-Based Anodes Operating at Reduced Temperatures. *Appl. Energ.* 164, 563–571. doi:10.1016/j.apenergy.2015.12.014

Rosa, D. L., Sin, A., Faro, M. L., Monforte, G., Antonucci, V., and Aricò, A. S. (2009). Mitigation of Carbon Deposits Formation in Intermediate Temperature Solid Oxide Fuel Cells Fed with Dry Methane by Anode Doping with Barium. *J. Power Sourc.* 193, 160–164. doi:10.1016/j.powersour.2009.01.096

Shimada, H., Li, X., Hagiwara, A., and Ihara, M. (2013). Proton-conducting Solid Oxide Fuel Cells with Yttrium-Doped Barium Zirconate for Direct Methane Operation. *J. Electrochem. Soc.* 160, F597–F607. doi:10.1149/2.079306jes

Shimonosono, T., Hirata, Y., Ehira, Y., Sameshima, S., Horita, T., and Yokokawa, H. (2004). Electronic Conductivity Measurement of Sm- and La-Doped Ceria Ceramics by Hebb?Wagner Method. *Solid State Ionics* 174, 27–33. doi:10.1016/j.ssi.2004.07.025

Simwonis, D., Tietz, F., and Stöver, D. (2000). Nickel Coarsening in Annealed Ni/8YSZ Anode Substrates for Solid Oxide Fuel Cells. *Solid State Ionics* 132, 24–251. doi:10.1016/S0167-2738(00)00650-0

Skalar, T., Jelen, E., Novosel, B., and Marinšek, M. (2016). Oxidation of Carbon Deposits on Anode Material Ni-YSZ in Solid Oxide Fuel Cells. *J. Therm. Anal. Calorim.* 127, 265–271. doi:10.1007/s10973-016-5671-8

Son, C. (2002). Fuel Processing for Low-Temperature and High-Temperature Fuel Cells: Challenges, and Opportunities for Sustainable Development in the 21st century. *Catal. Today* 77, 17–49. doi:10.1016/S0920-5861(02)00231-6

Wang, J. B., Jang, J.-C., and Huang, T.-J. (2003). Study of Ni-Samaria-Doped Ceria Anode for Direct Oxidation of Methane in Solid Oxide Fuel Cells. *J. Power Sourc.* 122, 122–131. doi:10.1016/S0378-7753(03)00438-5

Wright, J., and Virkar, A. V. (2011). Conductivity of Porous Sm2O3-Doped CeO2 as a Function of Temperature and Oxygen Partial Pressure. *J. Power Sourc.* 196, 6118–6124. doi:10.1016/j.jpowsour.2011.03.043

Yahiro, H., Eguchi, K., and Arai, H. (1989). Electrical Properties and Reducibilities of Ceria-Rare Earth Oxide Systems and Their Application to Solid Oxide Fuel Cell. *Solid State Ionics* 36, 71–75. doi:10.1016/0167-2738(89)90061-1

Yang, L., Choi, Y., Qin, W., Chen, H., Blinn, K., Liu, M., et al. (2011). Promotion of Water-Mediated Carbon Removal by Nanostructured Barium Oxide/nickel Interfaces in Solid Oxide Fuel Cells. *Nat. Commun.* 2, 357. doi:10.1038/ncomms1359

Zhang, X., Ohara, S., Maric, R., Mukai, K., Fukui, T., Yoshida, H., et al. (1999). Ni-SDC Cermet Anode for Medium-Temperature Solid Oxide Fuel Cell with Lanthanum Gallate Electrolyte. *J. Power Sourc.* 83, 170–177. doi:10.1016/S0378-7753(99)00293-1

**Conflict of Interest:** The authors declare that the research was conducted in the absence of any commercial or financial relationships that could be construed as a potential conflict of interest.

**Publisher's Note:** All claims expressed in this article are solely those of the authors and do not necessarily represent those of their affiliated organizations, or those of the publisher, the editors and the reviewers. Any product that may be evaluated in this article, or claim that may be made by its manufacturer, is not guaranteed or endorsed by the publisher.